Comprehensive modulation potential for the solar modulation of Galactic cosmic rays

Xiaojian Song and Xi Luo*
Shandong Institute of Advanced Technology (SDIAT), 250100 Jinan, Shandong, China

Marius S. Potgieter
Institute for Experimental and Applied Physics (IEAP), Christian-Albrechts University in Kiel, 24118 Kiel, Germany and Shandong Institute of Advanced Technology (SDIAT), 250100 Jinan, Shandong, China

Ming Zhang
Department of Physics and Space Sciences, Florida Institute of Technology, Melbourne, Florida 32901, USA

(Received 29 September 2022; accepted 18 November 2022; published 6 December 2022)

The concept of the modulation potential being utilized to describe the solar modulation of galactic cosmic rays is calculated based on the full three-dimensional Parker transport equation. This is in sharp contrast to the force-field approach, which is based on a series of approximations of this equation and where traditionally all the physical processes are condensed into a single parameter without knowing their relative contribution. In our comprehensive approach to the modulation potential, the contribution of all the different physical processes is given explicitly as derived directly from the parameters of Parker's transport equation. We use the stochastic differential equations approach to study the effects of each of these different physical modulation processes thoroughly and then also determine the rigidity and mass-to-charge-ratio (A/Z) of these processes for the first time in the context of a modulation potential. It is found that: (1) This comprehensive modulation potential for galactic cosmic particles with a given rigidity at the Earth is a random variable, which can be fit by an inverse Gaussian distribution; (2) the rigidity and A/Z dependence of this modulation potential can be divided into three categories based on the index value of power law diffusion; (3) the modulation caused by convection becomes weaker with increased rigidity and eventually dissipates, leading to a larger modulation potential for particles with a larger A/Z; (4) particle drift significantly reduces this modulation potential and its variation with changes in the tilt angle of the heliospheric current sheet has a distinct pattern for each of the two solar magnetic field polarities.

DOI: 10.1103/PhysRevD.106.123004

I. INTRODUCTION

Galactic cosmic rays (GCRs), when entering the heliosphere, are modulated by the disturbed solar wind and its embedded magnetic field so that their fluxes and spectral shapes change with the variation of solar activity, generally called solar modulation; for reviews, see Refs. [1–4]. It is known that these charged particles may cause radiation damage to spacecraft and even threaten the safety of astronauts in outer space [5]. The modulation processes are described by the well-known Parker transport equation [TPE; [6]]:

$$\frac{\partial f}{\partial t} = -(\boldsymbol{V}_{sw}+\boldsymbol{V}_d)\cdot\nabla f+\nabla\cdot(\boldsymbol{K}_s\cdot\nabla f)+\frac{1}{3}(\nabla\cdot\boldsymbol{V}_{sw})\frac{\partial f}{\partial \ln p}, \tag{1}$$

where $f(\boldsymbol{r}, p, t)$ is the GCR phase space density (PSD), $\boldsymbol{r}$ is heliocentric position, p is the momentum of these particles, and t is time. Here, $f(\boldsymbol{r}, p, t)$ is related to the differential intensity by $j(T) = p^2 f$, where T is a particle's kinetic energy per nucleon; $\boldsymbol{V}_{sw}$ is the solar wind velocity, $\boldsymbol{V}_d$ is the pitch angle averaged drift velocity, and $\boldsymbol{K}_s$ denotes the diffusion tensor. The terms on the right-hand side of Eq. (1) describe the four main physical processes: solar wind convection, particle drift in the global heliospheric magnetic field (HMF), diffusion because of irregularities in the HMF, and adiabatic energy losses caused by the expansion of the solar wind.

The widely used force-field approach for calculating a modulation potential [e.g., [7,8]] is based on several serious simplifications to the transport equation given above: (1) a steady state so that $\partial f/\partial t = 0$; (2) an adiabatic energy loss rate $dR/dt = (R/3)\boldsymbol{V}_{sw}\cdot\nabla f/f = 0$ with $R = pc/Ze$ the particle's rigidity in terms of momentum p, the speed of

*xi.luo@iat.cn

light c, the particle's charge Z with e the elementary charge; (3) no particle drifts; (4) a spherical symmetry which means the modulation process is essentially one-dimensional. This leads to:

$$\frac{V_{sw}R}{3}\frac{\partial f}{\partial R}+K_s\frac{\partial f}{\partial r}=0, \tag{2}$$

which is a first-order partial differential equation with solution

$$f_0(R_0)=f_b(R_b) \tag{3}$$

along contours of the characteristic equation

$$dR/dr=RV_{sw}/(3K_s) \tag{4}$$

in (r,R) space. The parameters with subscripts $0,b$ represent values at the position of the Earth and at the outer boundary of the modulation region, respectively. For convenience, in this paper, R_0 is called the start rigidity, and R_b the end rigidity. Thus, R_b-R_0 determines the GCR particles' rigidity loss due to the solar modulation process. Additionally, when it is assumed that the diffusion coefficient K_s has the form $K_s=\beta k_1(r)\cdot k_2(R)$, and with $k_2\propto R$, a straightforward solution for Eq. (4) is obtained:

$$\phi\equiv\frac{A}{Z}\int_{T_0}^{T_b}dT=\int_{R_0}^{R_b}\beta dR=\int_{r_0}^{r_b}\frac{V_{sw}}{3k_1}dr, \tag{5}$$

where A, T, R is the particle's mass, kinetic energy and rigidity; β is the ratio between the speed of the particle and that of light. Here, ϕ is called the solar modulation potential which denotes energy changes of GCRs from the heliopause (modulation boundary) to the Earth; the last part which contains the solar wind velocity, is the simplified form used as the so-called force-field parameter.

In the original force-field approach, ϕ was assumed to have the same value for different GCR species with a different start rigidity, and ϕ only changes with the solar activity [e.g., [9]]. Because of the assumption made in the derivation process, as mentioned above, the force-field approach can be used only in very limited circumstances. However, in applications these limitations have soon become neglected, so that all the physical processes in the heliosphere have been assumed to be condensed in this single parameter, without a detailed demonstration of what it actually means, especially in the literature of an experimental nature, probably because of its simplicity. In practice, the parameter ϕ is calculated by an intricate inversion process using Eq. (3). For example, with the PSD of observational GCR data and their local interstellar spectra (LIS's), the value of R_b is obtained and related to ϕ by [refer to Eq. (5)]:

$$R_b=\sqrt{R_0^2+\phi^2+2R_0\phi\sqrt{1+\left(\frac{Ae_0}{ZR_0}\right)^2}}, \tag{6}$$

where e_0 is the nucleon rest energy. Here, ϕ is an intrinsic property of solar modulation conditions in the heliosphere and should only relate to the heliospheric environment, but this inversion process includes uncertainties in observational GCR data and in their corresponding LIS's. Reference [10] found that the ϕ calculated by using various LIS's [e.g., [11–14]] differ with each other significantly and seems inadequate to use for such purposes. In recent years, a number of authors presented a rigidity dependence of ϕ to phenomenologically fit the observational data at the Earth [e.g., [15–17]]. In addition, Refs. [18,19] incorporated the effects of particle drift into ϕ. All these modifications allow for some additional freedom in reproducing observed GCR spectra at the Earth while attempting to maintain the simplicity of the force-field model. However, they do not address the physical mechanism in terms of heliospheric modulation processes underneath this type of required freedom.

It is evident from what we describe above that several questions about this approach come forward (some may even be seen as objections to the force-field approach and the way it has been applied lately) e.g., what becomes of the expression for a modulation potential without any simplification? And, is there any rigidity and A/Z dependence of the modulation potential? What are the effects of the three major and quite different physical processes on such a modulation potential? What we present below, is a detailed study of these questions in an effort to resolve them and to understand what the implications are for solar modulation in terms of a modulation potential. We start off with a set of stochastic differential equations (SDE) that are equivalent to the TPE, similar to what we had used before and then make some modifications in order to numerically calculate what may be called a comprehensive modulation potential as is shown in Sec. II. The influences of the various physical processes on this modulation potential and their rigidity and A/Z dependence are presented and discussed in Sec. III. We consider these results in the context of a modulation potential as new, not obtainable through the force-field approach as it based on too many simplifying assumptions. In conclusion, a summary and discussions are given in Sec. IV.

II. A COMPREHENSIVE MODULATION POTENTIAL

For a pseudoparticle with rigidity R at position $\boldsymbol{r}$, the SDE equivalent to the TPE has the form:

$$d\boldsymbol{r}=(\nabla\cdot\boldsymbol{K}_s-\boldsymbol{V}_{sw}-\boldsymbol{V}_d)ds+\sqrt{2\boldsymbol{K}_s}\cdot d\boldsymbol{W}(ds), \tag{7}$$

$$dR = \frac{1}{3}R(\nabla \cdot \boldsymbol{V}_{sw})ds, \tag{8}$$

where s is the backward time and $ds = -dt$, each elements in $\boldsymbol{dW}$ satisfy a Gaussian distribution of zero mean and a variance of ds. By comparing with the characteristic equation of the force-field approach [Eq. (4)], Eq. (7) is regarded as the characteristic equation of the TPE without any simplification. For detailed discussions of this approach to solar modulation, see Ref. [e.g., [20–23]].

Adopting that $d\phi = A/ZdT = \beta dR$ and utilizing Eq. (8), it is obtained that $d\phi = \beta R\nabla \cdot \boldsymbol{V}_{sw}ds/3$, which is then used to substitute the independent variable ds in Eq. (7):

$$d\boldsymbol{r} = \frac{3(\nabla \cdot \boldsymbol{K}_s - \boldsymbol{V}_{sw} - \boldsymbol{V}_d)}{\beta R\nabla \cdot \boldsymbol{V}_{sw}}d\phi + \sqrt{\frac{6\boldsymbol{K}_s}{\beta R\nabla \cdot \boldsymbol{V}_{sw}}} \cdot d\boldsymbol{W}(d\phi). \tag{9}$$

This equation describes typical Brownian motion with three "drift" terms:

$$\boldsymbol{V}_{\phi,\mathrm{diff}} = \frac{3\nabla \cdot \boldsymbol{K}_s}{\beta R\nabla \cdot \boldsymbol{V}_{sw}}, \tag{10}$$

$$\boldsymbol{V}_{\phi,\mathrm{conv}} = -\frac{3\boldsymbol{V}_{sw}}{\beta R\nabla \cdot \boldsymbol{V}_{sw}}, \tag{11}$$

$$\boldsymbol{V}_{\phi,\mathrm{drift}} = -\frac{3\boldsymbol{V}_d}{\beta R\nabla \cdot \boldsymbol{V}_{sw}}. \tag{12}$$

Note that $\boldsymbol{V}_{\phi,\mathrm{diff}}$, $\boldsymbol{V}_{\phi,\mathrm{conv}}$, and $\boldsymbol{V}_{\phi,\mathrm{drift}}$ are not real velocities, the actual units are AU/GV. They represent the "drift" terms in the modified SDE [Eq. (9)] and relate to diffusion, convection and drift in Parker's original TPE.

In Eq. (9), with the increase of ϕ in the SDE approach that we utilized, the pseudo-particle moves toward the heliopause from the Earth. The modulation potential can be considered as the value of ϕ when a pseudoparticle first hit the heliopause, to be called the first hitting potential. The stochastic term, $d\boldsymbol{W}$, causes each particle to have a different trajectory and the first hitting potential is path dependent, especially in 3D, see Ref. [24]. So that the first hitting potential is not a definite value, but a random variable, e.g., considering GCR protons with a certain rigidity under the same heliospheric environment, the energy loss for different pseudoparticles may be distinct from each other [e.g., [25,26]].

Mathematically, the first hitting time for these particles, which undergo simple (one-dimension, constant drift and diffusion) Brownian motion, should obey an inverse Gaussian function [e.g., [27] and referring to the Appendix]. In the next section, it is shown that the distribution of the first hitting potential in Eq. (9) calculated numerically in 3D can also be well fitted by an inverse Gaussian function:

$$IG(\phi, \Lambda, \phi_{\mathrm{avg}}) = \sqrt{\frac{\Lambda}{2\pi\phi^3}}\exp\left\{\frac{-\Lambda(\phi - \phi_{\mathrm{avg}})^2}{2\phi_{\mathrm{avg}}^2\phi}\right\}, \tag{13}$$

where ϕ_{avg} is the mean value of ϕ; Λ determines the distribution of ϕ on both sides of ϕ_{avg}. By comparing with the solution given in the Appendix, ϕ_{avg} should be inversely proportional to the first part on the right hand side of Eq. (9) ("drift" term) and Λ is determined by the second term of Eq. (9) (stochastic term).

A. Heliospheric parameters

Based on observational facts, the solar wind velocity $\boldsymbol{V}_{sw}$ is (1) radially accelerating from zero to a steady value within 0.3 AU from the Sun [28]; (2) during solar minimum period, $\boldsymbol{V}_{sw}$ increases from ~400 km/s in the equatorial plane to ~800 km/s at high heliolatitude [29]; (3) there is no clear latitude dependency during solar maximum period [e.g., [1], and references there in]. The solar wind velocity in the whole heliosphere can be expressed as [e.g., [1,2,30,31]]:

$$\boldsymbol{V}_{sw} = V_0\left\{1 - \exp\left[\frac{40}{3}\left(\frac{r_s - r}{r_0}\right)\right]\right\} \times \left\{1.475 \mp 0.4\tanh\left[6.8\left(\theta - \frac{\pi}{2} \pm \xi\right)\right]\right\}\boldsymbol{e}_r, \tag{14}$$

where V_0 is related to the solar wind speed observed near the Earth, $r_s = 0.005$ AU is the radius of the Sun, $r_0 = 1$ AU, $\xi = \alpha + 15\pi/180$, and α is the tilt angle of the wavy heliospheric current sheet (HCS). The top and bottom signs correspond to the northern and southern hemisphere, respectively.

The heliospheric magnetic field (HMF) exhibits an archimedean spiral shape [32], which results from the rotation of the Sun. However, excessive GCR drift effects in the polar regions of the heliosphere will be caused by the standard Parker HMF, so that some efforts have been made to modify the classical Parker HMF [e.g., [1,33–35]]. In this context, Ref. [36] suggested a small latitudinal component to the standard Parker HMF in order to keep the magnetic field divergence free, and this simple modification can be expressed as:

$$\begin{aligned}\boldsymbol{B} &= \frac{A_s B_0}{r^2}(\boldsymbol{e}_r + \xi\boldsymbol{e}_\theta - \Psi\boldsymbol{e}_\varphi) \times [1 - 2H(\theta - \theta')],\\ \xi &= \frac{r\delta_m}{r_s \sin\theta},\\ \Psi &= \frac{(r - r_s)\sin\theta\Omega}{V_{sw}},\end{aligned} \tag{15}$$

where B_0 is related to the HMF observed near the Earth, A_s denotes the polarity of HMF with positive (negative) sign representing the HMF points outward (inward) in the northern hemisphere of the Sun, $\Omega = 2.66 \times 10^{-6}$ rad/s is the rotation speed of the Sun, and H is the Heaviside function. δ_m is set to be 2×10^{-5} [e.g., [4,35]]. To avoid a singularity, $\delta_m/\sin\theta$ is set equal to the value $\delta_m/\sin(1°)$ when $\theta < 1°$ or $\theta > 179°$.

The HCS latitudinal extent θ' introduced by Ref. [37,38] can be written as

$$\theta' = \frac{\pi}{2} - \arctan\left[\tan\alpha \sin\left(\varphi + \frac{\Omega(r - r_s)}{V_{sw}}\right)\right]. \quad (16)$$

See also the related discussions by Ref. [2,39].

B. Diffusion and Drift Coefficients

It is assumed that the diffusion of GCRs is caused by irregularities in the HMF on a small scale. Several theories have been developed over the years to describe the fundamental properties of diffusion [e.g., [40–45]]. However, there are still some obstacles to overcome for directly adapting these complicated theories into numerical models. In this work, for a clear description, the widely used empirical formula [30,46,47] is changed to:

$$\begin{aligned} K_{\parallel} &= K_0 \beta k_1(r) k_2(R), \\ k_1 &= B_{\rm eq}/B, \\ k_2 &= \begin{cases} (R/R_k)^b & R < R_k \\ (R/R_k)^c & R \geq R_k \end{cases} \end{aligned} \quad (17)$$

where K_0 is a constant in units of 10^{20} cm^2 s^{-1}, and with the rest of the equation written to be dimensionless. Here $B_{\rm eq}$ is the magnitude of the HMF measured near the Earth. This equation consists of two power laws; the slope of the rigidity dependence is determined by b and c when the particle's rigidity is below or above turnover point, R_k, respectively. As for the two perpendicular diffusion coefficients, they are scaled to the parallel diffusion coefficient by $K_{\perp,r} = 0.02 K_{\parallel}$ and $K_{\perp,\theta} = \{2 + \tanh[8(|\theta - 90°| - 35°)]\} K_{\perp,r}$, which comes from Refs. [30,48]. Though some uncertainty exist in these simplified scaling relations [47,49], it is enough to study their influence on the rigidity and A/Z dependence of modulation.

The drift velocity of charged particles caused by the curvatures, gradients and a current sheet in the large scale HMF can be expressed as:

$$\boldsymbol{V}_d = K_{A0} \frac{qR\beta}{3} \nabla \times \left(\frac{\boldsymbol{B}}{B^2}\right), \quad (18)$$

where K_{A0} is a constant, ranging from 0 to 1, with $K_{A0} = 1$ describing full drift; q is the particles' charge-sign; see also the discussion by Ref. [30].

C. Numerical solutions

As a sample, the numerical result of Eq. (9) for a particle with $A/Z = 1$ is shown in Fig. 1 under the condition of $V_0 = 400$ km/s, $B_0 = 5$ nT, $A_s > 0$, and $\alpha = 20°$. Following recent numerical simulation studies [e.g., [49,50]], the diffusion and drift parameters are set to be $b = 0.7, c = 2.0, R_k = 4$ GV, $K_0 = 400$, and $K_{A0} = 1$. The top left panel shows the colored contour plot of the probability distribution function (PDF) of the first hitting potential, ϕ, with a different start rigidity, R_0. The histograms in the other three panels are the cross section at $R_0 = 0.1, 1$, and 10 GV, respectively. It is evident from Figs. 1(b)–1(d) that the PDF of ϕ is not symmetrical, it drops rapidly near 0 and drops slowly when approaching a large value, forming a long right-hand tail. The black dashed lines are the best fit to the PDF using the inverse Gaussian function as described in Eq. (13), the best-fit parameters are labeled in each panel. With the increase of R_0, the average value of $\phi_{\rm avg}$ decreases sharply when $R_0 < 0.1$ GV, decreases slowly or remains unchanged in the range of 0.1 GV $< R_0 <$ 4 GV, and decreases sharply again to nearly 0 when $R_0 > 4$ GV; the variation of Λ (denoting the dispersion of ϕ on both sides of $\phi_{\rm avg}$) is mainly similar to that of $\phi_{\rm avg}$. The upper abscissa (red fonts) in Fig. 1(b)–1(d) shows the end rigidity, R_b, corresponding to the value of ϕ in the lower abscissa one-by-one through Eq. (6). It can be seen that, with the increase of ϕ from 0 GV to 1 GV, R_b changes from 0.1 GV to 1.7 GV ($\sim$170%) when $R_0 = 0.1$ GV; but when $R_0 = 10$ GV, R_b merely increases from 10 GV to 11 GV ($\sim$10%). Thus, the same variation of ϕ corresponds relative large change of R_b as the start rigidity of R_0 is low. The right Y axis shows the phase space density (PSD) of the GCR proton LIS [49] at different R_b. The large relative change of R_b at low R_0 leads to the fast decrease of the PSD.

Based on the SDE approach, the observational PSD is an average of the LIS PSD with a different modulation potential, which can be described by the first two terms in the following formula:

$$\int f_b(R_b) IG(\phi) d\phi = f_0(R_0) = f_b(R_{b,\rm eff}), \quad (19)$$

where $IG(\phi)$ denotes the inverse Gaussian distribution of ϕ [Eq. (13)]. The last two terms are usually used to calculate the conventional modulation potential $\phi_{\rm eff}$ (as described in Sec. I), which is related to $R_{b,\rm eff}$ by Eq. (6). Considering only the first and last terms, $\phi_{\rm eff}$ can be derived from the distribution of ϕ and the LIS directly without observational data. The red curve in Fig. 1(a) and red vertical lines in Figs. 1(b)–1(d) show $\phi_{\rm eff}$ calculated by using the above method. It follows that, when R_0 is large enough (> 4 GV), $\phi_{\rm eff}$ and $\phi_{\rm avg}$ are almost equal to each other; when R_0 is

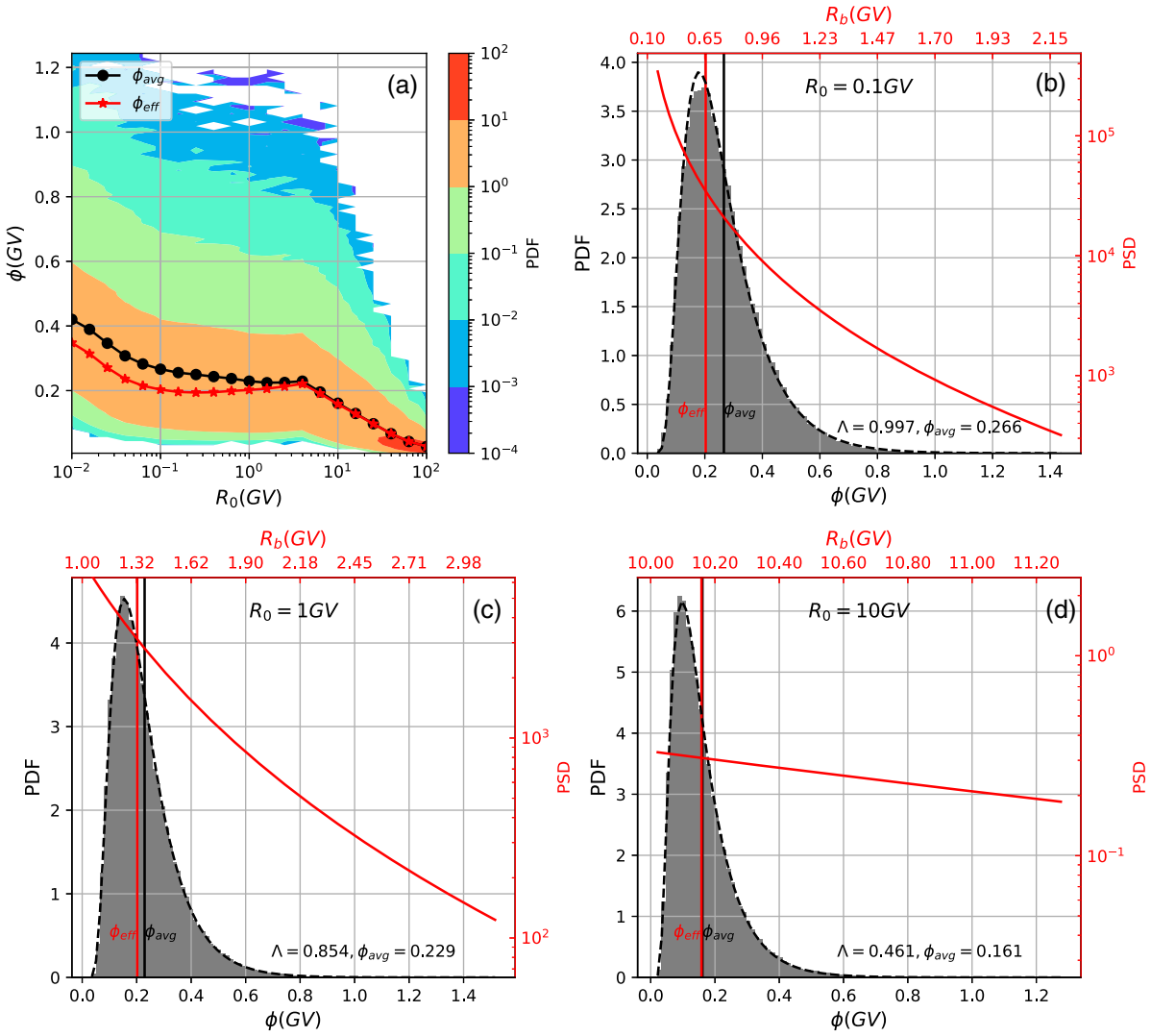

FIG. 1. The numerical result of Eq. (9) under the conditions as described in Sec. II C for GCR particles with $A/Z = 1$. Panel (a): Probability distribution function (PDF) of ϕ with a different start rigidity R_0. The black (red) line is the average value (effective value, refer to Sec. II C) of ϕ. Panels (b,c,d): Histograms of ϕ when $R_0 = 0.1$, 1, 10 GV, respectively; black dashed lines are the best fit to histogram using the inverse Gaussian function with best-fit parameters labeled in each panel. The upper axes (in red) show the end rigidity, R_b, which corresponding to ϕ one-by-one. The red curves show the phase space density (PSD) of the LIS at different end rigidity.

small (< 4 GV), as the PSD of the LIS at low ϕ is much higher than that at large ϕ, $\phi_{\rm eff}$ is less than $\phi_{\rm avg}$.

III. CONTRIBUTIONS OF VARIOUS PHYSICAL PROCESSES

The distribution of ϕ is determined by Λ and $\phi_{\rm avg}$; with Λ controlling the dispersion of ϕ and relying solely on the diffusion process. And $\phi_{\rm avg}$ is the average value of ϕ and relies on the three main physical processes (diffusion, convection, drift), it changes greatly with solar activity. Also, as shown in Fig. 1, $\phi_{\rm avg}$ is the main factor in determining the GCR fluxes at the Earth. The influence of the three main physical processes on the rigidity and A/Z dependence of $\phi_{\rm avg}$ is studied in this section. See Sec. II C for the parameters' setup in our numerical model.

A. The diffusion effect

As shown in Eq. (17), the diffusion tensor is considered to have separable terms, see also [e.g., [50,51]]. Therefore Eq. (10) can be rewritten as:

$$\boldsymbol{V}_{\phi,\rm diff} = K_0 \frac{3\nabla\cdot\boldsymbol{k}_1}{\nabla\cdot\boldsymbol{V}_{sw}}\frac{k_2}{R}. \tag{20}$$

Since $\boldsymbol{k}_1$ and $\boldsymbol{V}_{sw}$ is not related to the particle's rigidity, considering only the diffusion process, the rigidity and A/Z

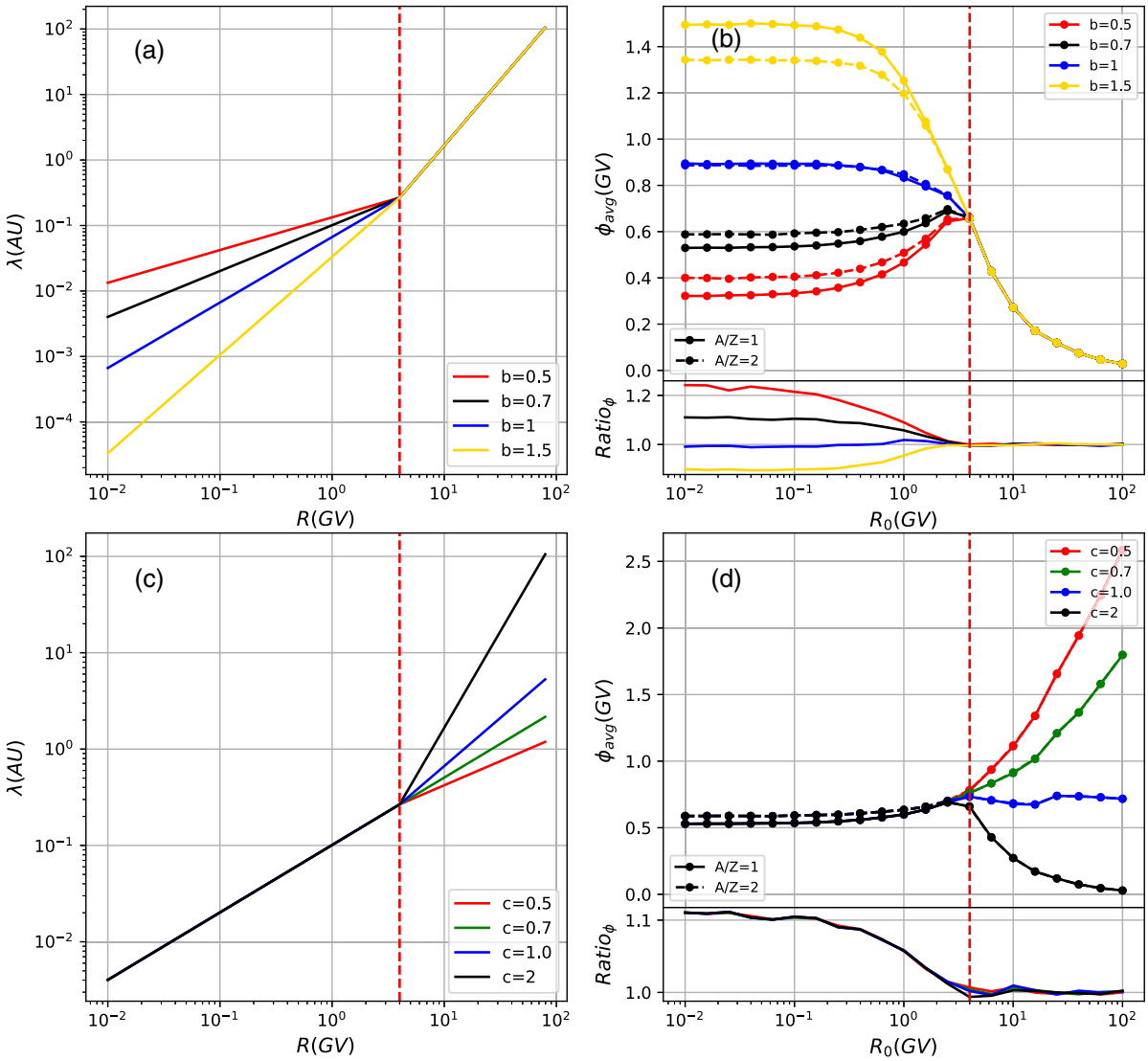

FIG. 2. The effect of the SDE diffusion term $\nabla \cdot \boldsymbol{K}_s$ on the ϕ_{avg}. Panel (a): MFPs calculated with four different rigidity power indices b [in Eq. (17)] below 4 GV with other parameters unchanged (refer to Sec. II C). Panel (b): Corresponding ϕ_{avg} for $A/Z = 2$ (dashed lines) and $A/Z = 1$ (solid lines); the lower part shows the corresponding color coded ratios. Panels (c,d) are similar to panels (a,b) but with results focused on four different power indices c above 4 GV.

dependence of ϕ_{avg} only relate to the power law index of the rigidity variable contained in function k_2.

Figures 2(a) and 2(c) show the mean free paths (MFP) λ, in units of AU, of GCR particles and relate to the diffusion coefficient (DC) by $K_s = \lambda\beta c/3$. The slope of the MFP indicates the power law index of k_2 as a function of rigidity. The black lines are plotted using the same parameters as described in Sec. II C. Figures 2(a) and 2(c) focus on the power index at low and high rigidity, respectively, with the other parameters unchanged. Figures 2(b) and 2(d) show the corresponding ϕ_{avg} for $A/Z = 2$ (dashed lines) and $A/Z = 1$ (solid lines) with the corresponding color coded MFPs shown in Figs. 2(a) and 2(c). The blue lines in all four panels are the equivalent of what is usually applied in the force-field approach. The general trends in this figure are discussed as follows:

(1) The larger the MFP (or DC) becomes, the smaller the value of ϕ_{avg}. As shown in Eq. (20), a larger DC leads to a larger $\boldsymbol{V}_{\phi,\text{diff}}$. Correspondingly, the modulation potential for a particle approaching the heliopause in Eq. (9) is reduced. In Figs. 2(a) and 2(b), the MFP with $b = 0.5$ (red line) is larger than that with $b = 1.5$ (yellow line), whereas ϕ_{avg} with $b = 0.5$ is less than that with $b = 1.5$. (However, note how ϕ_{avg} levels off at low rigidity despite that the MFP is systematically decreasing, which will be discussed next). Similarly, in Figs. 2(c) and 2(d), the MFP with $c = 0.5$ (red line) is lower than that with $c = 2$

(black line), whereas $\phi_{\rm avg}$ with $c = 0.5$ is larger than that with $c = 2$.

(2) The rigidity dependence of $\phi_{\rm avg}$ becomes insignificant for all cases when $R_0 < 0.1$ GV. It follows from Eq. (6) that when $R_0 \ll \phi_{\rm avg}, e_0$, the rigidity of the considered GCR particles moving through the heliosphere is almost independent on R_0. So, for particles with a different start rigidity, they have the nearly same $\boldsymbol{V}_{\phi,\rm diff}$, and eventually the same $\phi_{\rm avg}$, as shown in the left side of Fig. 2(b).

(3) The rigidity dependence of $\phi_{\rm avg}$ when $R_0 > 0.1$ GV clearly depends on the power law index of the MFPs.

If the power index is equal to 1 in Eq. (20), $\boldsymbol{V}_{\phi,\rm diff}$ becomes independent of the particle's rigidity, which leads to the independence of $\phi_{\rm avg}$ on R_0 [the blue lines in Figs. 2(b) and 2(d)]. Note that the end rigidity of some particles with $R_0 = 1$ GV may exceed the turn over rigidity R_k; the large power index at higher rigidity range ($R > R_k$) leads to the decrease of the blue line in Fig. 2(b) as $R_0 > 1$ GV. If the power index is smaller than 1, $\boldsymbol{V}_{\phi,\rm diff}$ is anti correlated with the particle's rigidity, which leads to the positive correlation between $\phi_{\rm avg}$ and R_0 [the red lines in Figs. 2(b) and 2(d)]; if the power index is bigger than 1, $\boldsymbol{V}_{\phi,\rm diff}$ is positively correlated with the particle's rigidity, which leads to the anti correlation between $\phi_{\rm avg}$ and R_0 [the yellow line in Fig. 2(b) and black line in Fig. 2(d)].

(4) There is hardly any A/Z dependence of $\phi_{\rm avg}$ when $R_0 > 4$ GV. It follows from Eq. (6) that if $R_0 \gg e_0$, the rigidity of particles moving through the heliosphere is almost no longer changing with A/Z. Particles with different A/Z have the same $\boldsymbol{V}_{\phi,\rm diff}$, and eventually the same averaged solar modulation potential [as shown on the right side of Fig. 2(d)].

(5) The A/Z dependence of $\phi_{\rm avg}$ when $R_0 < 4$ GV depends on the power law index of the MFPs.

If the power index is equal to 1, $\boldsymbol{V}_{\phi,\rm diff}$ becomes independent of rigidity and A/Z. The blue line in lower panel of Fig. 2(b) remains almost along the line with $\text{Ratio}_\phi = 1$. The rigidity of particles with the same R_0 and ϕ is positively correlated with A/Z. If the power index is smaller than 1, $\boldsymbol{V}_{\phi,\rm diff}$ is anti correlated with the particle's rigidity, so, bigger A/Z leads to larger $\phi_{\rm avg}$ [the red lines in Fig. 2(b)]; If the power index is more than 1, $\boldsymbol{V}_{\phi,\rm diff}$ is positively correlated with the particle's rigidity, larger A/Z leads to smaller $\phi_{\rm avg}$ [the yellow line in Fig. 2(b)].

B. The convection effect

In order to study this aspect, based on the adapted solar wind model [Eq. (14)], Eq. (11) can be rewritten as follows:

$$\boldsymbol{V}_{\phi,\rm conv} = -\frac{3}{2}\frac{\sqrt{R^2 + (Ae_0/Z)^2}}{R^2}\boldsymbol{r}. \tag{21}$$

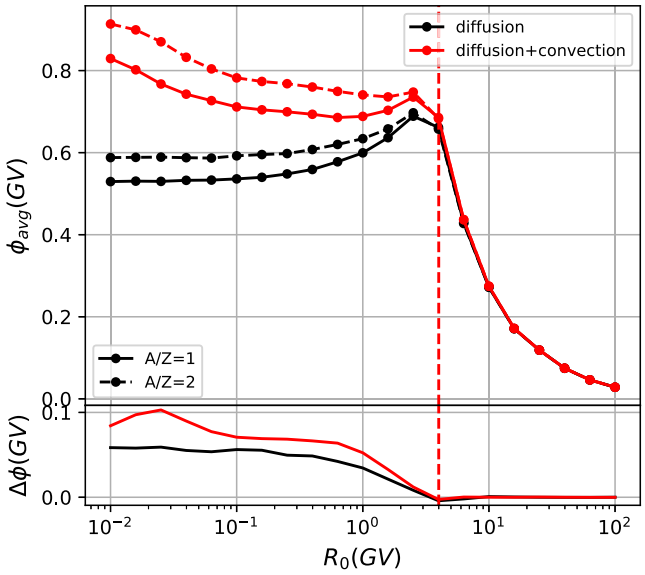

FIG. 3. The influence of the SDE convection term on $\phi_{\rm avg}$. As a comparison, the black lines show the result of Eq. (9) containing only the diffusion term whereas the red lines show the results with the convection term added. Dashed and solid lines are the results for $A/Z = 2$ and $A/Z = 1$, respectively, with their differences shown in the lower panel.

This expression contains R and A/Z explicitly, which means that the convection related SDE term [Eq. (11)] also contributes to the rigidity and A/Z dependence of $\phi_{\rm avg}$. The black lines in Fig. 3 show $\phi_{\rm avg}$ calculated solely considering diffusion whereas the red lines exhibit the addition of convection. It follows that:

(1) The convection term modifies the modulation potential.

The value of $\boldsymbol{V}_{\phi,\rm conv}$ is negative, which means that the convection process hinders the motion of GCRs into the heliosphere differently than the diffusion process. The pseudoparticles in our SDE approach need a larger modulation potential to propagate between the heliopause and the Earth.

(2) The modification decreases with increasing R_0, and dissipates around $R_0 = 4$ GV. Since $\boldsymbol{V}_{\phi,\rm conv}$ is anti-correlated with rigidity, its effect is weakened with higher rigidity. On the other hand, in our numerical model the diffusion process becomes stronger as the rigidity increases. Therefore, the effect of convection dissipates and becomes insignificant when comparing with the diffusion effect.

(3) The modification is larger as values of A/Z increases.

The lower panel of Fig. 3 shows the difference between $\phi_{\rm avg}$ calculated for $A/Z = 2$ (dashed lines) and for $A/Z = 1$ (solid lines). It can be seen that the convection process significantly enhances the modulation potential for particles with larger A/Z. This effect can be explained by the correlation between $\boldsymbol{V}_{\phi,\rm conv}$ and A/Z.

C. The effect of drift

Equation (12) can be rewritten to be

$$\boldsymbol{V}_{\phi,\mathrm{drift}} = -K_{A0}\frac{q\nabla\times(\boldsymbol{B}/B^2)}{\nabla\cdot\boldsymbol{V}_{sw}}. \tag{22}$$

In this equation the described effect is charge-sign dependent but independent of R, and as such only relates to the heliospheric environment, e.g., the HCS tilt angle α, the solar magnetic field and its polarity A_s. This means that the SDE drift term does not contribute to the rigidity or A/Z dependence of ϕ_{avg}.

Figure 4(a) shows the comparison of ϕ_{avg} calculated without (black line) and with (colored lines) this drift term for GCR particles with $A/Z = 1$. To study the effect of the drift term, the simulation is carried out under a positive solar magnetic polarity ($A_s > 0$) and using different HCS tilt angles (α) (colored lines). As it is demonstrated, the colored lines are all below the black line, which means that this drift term effectively promotes the motion of GCRs in the heliosphere. At high enough rigidity, drift effect becomes insignificant when comparing with the diffusion effect, so that all lines converge.

In order to illustrate the impact of α on ϕ_{avg}, Fig. 4(b) shows the variation of ϕ_{avg} with the increase of α for particles with $R_0 = 1$ GV. It follows that when $\alpha = 0$ (solar minimum activity), the contribution of this term to ϕ_{avg} is significantly smaller than without it whereas an increasing α systematically increases ϕ_{avg} to become closer to the value without drift. Figures 4(c) and 4(d) are similar to Figs. 4(a) and 4(b) but for a negative magnetic polarity ($A_s < 0$). Evidently, the drift term also reduces the modulation potential but differently and less compared with when $A_s > 0$. In Fig. 4(d) it is shown how the increase rate

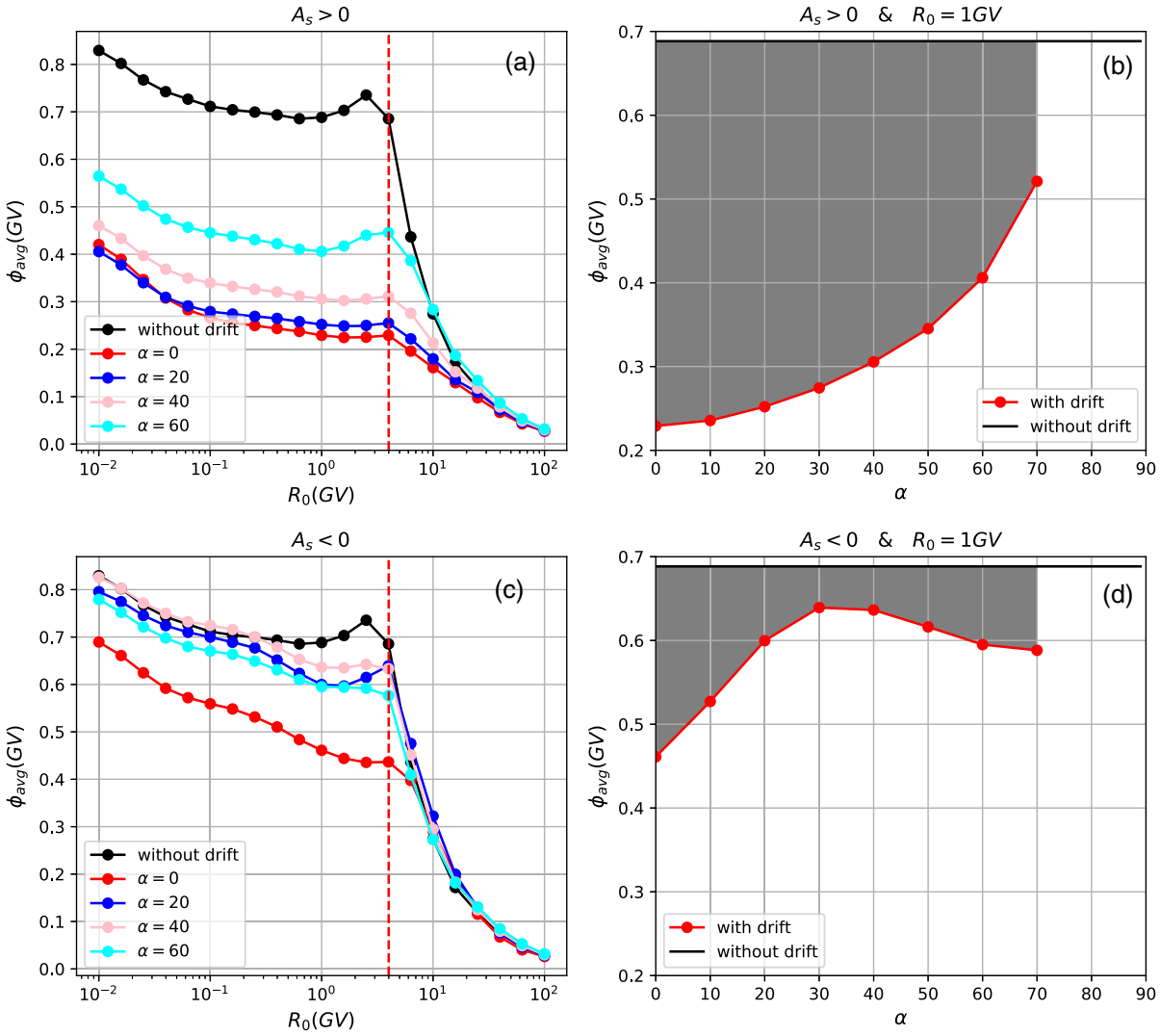

FIG. 4. The influence of the SDE drift term on ϕ_{avg}. Panel (a): Black line shows the result of Eq. (9) without this drift term; the colored lines show the results with the drift term using increasing tilt angles of the HCS when the magnetic polarity is $A_s > 0$. Panel (b): Variation of ϕ_{avg} with increasing tilt angles for particles with $R_0 = 1$ GV when $A_s > 0$. Panels (c,d): Similar to (a,b) but for $A_s < 0$.

of $\phi_{\rm avg}$ with increasing α is getting smaller to eventually levels off and even showing a slight decline.

IV. DISCUSSION, SUMMARY AND CONCLUSION

Traditionally, the simplified modulation potential, last part in Eq. (5), has been considered to condense all physical processes in the heliosphere into a single parameter, see e.g. Ref. [19], a controversial assumption because it was unknown what the relative contributions of these physical processes really were. A real drawback was that its rigidity and A/Z dependence, two crucial features of the solar modulation of GCRs, were undetermined. In fact, the simplified modulation potential as applied over the years has almost never been related to any specific underlying modulation processes [8]. In this work, the widely used SDE approach to solar modulation is applied to address these shortcomings by performing a thorough investigation on what we called a comprehensive modulation potential for GCRs.

The numerical results show that the modulation potential ϕ for particles with a given rigidity at 1 AU (at Earth) is not a definite value, but a random variable and its distribution can be fitted by an inverse Gaussian function. This result is not new, it is consistent to how it has been understood and reported in most publications on solar modulation. The traditional one-parameter modulation potential describes not the effect on the energy change of every single particle but the effective energy change out of a distribution of values for that energy change. As the PSD of this LIS at low rigidity is much larger than it is at high rigidity, there are some differences between $\phi_{\rm eff}$ and $\phi_{\rm avg}$ (the average value of ϕ) at a low start rigidity, but the difference becomes negligible at a high start rigidity. The essential expressions on how the modulation processes are described in this SDE approach are given by Eqs. (9)–(12), which should be kept in mind in the discussion that follows. Of course, our discussion will show that the main features of this comprehensive modulation potential relate quite well to what is known from other and our own numerical studies when the TPE is solved in 3D, that is, not considering any kind of modulation potential.

It follows that how exactly diffusion is treated can be considered as the main determining factor that governs the transport of GCRs in the heliosphere; Fig. 2 illustrates how crucial its assumed rigidity power law index is for the rigidity and A/Z dependence of $\phi_{\rm avg}$. In this context, turbulence theory [see e.g., [43,44,52,53]] indicates that the power index increases from less than 1 at low rigidity to more than 1 at high rigidity. Several numerical simulations [e.g., [46,49,50,54]] report that the power law index at low and high rigidity can change from less than 1 to more than 1 under different levels of solar activity. In principle, different preset rigidity dependence may be used to determine $\phi_{\rm eff}$ and all may fit the measurements at Earth quite well when utilizing the uncertainty of the LIS's and in observational GCR spectra. Reference [16] reported how $\phi_{\rm eff}$ systematically decreases between 1 GV and 10 GV, a pattern that relates to the blue and yellow lines in Fig. 2(b), corresponding to a power law index in diffusion of $b \geq 1$ & $c > 1$. Reference [17] reported $\phi_{\rm eff}$ increasing slightly at first and then decreasing sharply between 1 GV and 10 GV, a pattern that relates to the black and red lines in Fig. 2(b), which corresponds to a power law index for diffusion of $b < 1$ & $c > 1$.

It follows that how convection is handled in determining $\phi_{\rm avg}$ can change it significantly for low rigidity particles and enhancing it for particles with larger A/Z, an effect that could not been studied in detail in the simplified potential approach or for other empirical expressions of $\phi_{\rm eff}$.

Including particle drift in determining $\phi_{\rm avg}$ reduces this modulation potential for both magnetic field polarities, significantly more so for a positive than a negative polarity. It seems that the results of the phenomenological fitting equation for $\phi_{\rm eff}$ given by Ref. [18] is basically consistent to our result, as the fitting process was design to be.

It is well known since the late 1980s [e.g., [55,56]] that the observed GCR flux at the Earth decreases progressively slower with an increasing HCS tilt angle α under $A_s < 0$ polarity conditions. See also the discussions of these effects done with SDE models by Refs. [39,57]. It is expected that the modulation potential should exhibit the same features, which in fact is the case as shown in Fig. 4(d). Under $A_s > 0$ polarity conditions, the decrease rate of GCR flux at the Earth is expected to systematically increase with increasing α, corresponding to our results shown in Fig. 4(b). In our work, to show the drift effect explicitly, we assume $K_{A0} = 1$ (maximum drifts) for all α. In most numerical simulations it is assumed that K_{A0} should decrease to 0 when α approaches very large values during solar maximum conditions [e.g., [46,47,58]]. This means that $\phi_{\rm avg}$ should also approach the value without drift for larger HCS tilt angles as follows from Fig. 4.

In summary, by utilizing the stochastic differential equation approach to solar modulation based on Parker's full transport equation, we calculated a generalized and comprehensive modulation potential for the heliospheric environment and found that: (1) This modulation potential for particles with a given rigidity at the Earth is a random variable which can be fit by an inverse gaussian distribution. (2) The rigidity and A/Z dependence of this modulation potential can be divided into three categories related to the index value of power law diffusion. (3) The modification caused by convection becomes weaker with increased rigidity and eventually dissipates; this leads to a larger modulation potential for particles with a larger A/Z. (4) Including particle drift significantly reduce the modulation potential; how this changes with the tilt angle of the heliospheric current sheet has distinct different patterns for the two solar magnetic field polarity epochs.

A final remark: It is evident that the main features of this computed comprehensive modulation potential relate quite well to what is known from comprehensive numerical

studies when the full TPE is solved (not the potential approach) using similar heliospheric parameters. We do not propose that our approach as presented here can replace the latter but as such it does connect the complicated TPE and easy understanding modulation potential concept. Our results complement the force-field approach, not just in terms of the actual values of ϕ but also in the interpretations of what they actually mean in the context of solar modulation. Perhaps, this can be taken as a warning against the use of the force-field approach to interpret high quality observations. It surely allows for a direct comparison with simplified modulation potential approaches, in particular the force-field approach as related to what was shown in Fig. 2, let alone what are presented in Figs. 3 and 4. The results in these two figures are beyond what the force-field approach can offer in terms of a modulation potential.

ACKNOWLEDGMENTS

The present work is jointly supported by the startup fund of Shandong Institute of Advanced Technology No. 2020106R01, Taishan Scholar Project of Shandong Province No. 202103143, and NSFC Grants No. U2106201, No. 41774185, No. U1738128, No. 41731067, and No. 18611640. We are grateful for the important discussion with Professors Fengsi Wei, Xueshang Feng, and Weiwei Xu.

APPENDIX: FIRST HITTING TIME PROBLEM

The one-dimension Brownian motion process $x(t)$ with constant drift (μ) and diffusion (σ) is defined by the following SDE:

$$dx(t) = \mu dt + \sigma dW(dt), \tag{A1}$$

with initial value x_0. Set $H_{x_b} = \inf(t|x(t) = x_b)$ denotes the first hitting time for the boundary $x_b > x_0$.

The corresponding partial differential equation to Eq. (A1) is

$$\frac{\partial p(x,t)}{\partial t} = -\mu \frac{\partial p(x,t)}{\partial x} + \frac{1}{2}\sigma^2 \frac{\partial^2 p(x,t)}{\partial x^2}, \tag{A2}$$

with the following initial and boundary value conditions:

$$p(x,0) = \delta(x - x_0); \qquad p(x_b,t) = 0, \tag{A3}$$

where $p(x,t)$ is the probability density for the stochastic variable $x(t)$ to have a value x at time t.

This boundary value problem can be solved using the standard method of images technique and the solution is described by:

$$p(x,t) = \frac{1}{\sqrt{2\pi\sigma^2 t}}\left\{\exp\left[-\frac{[x-\mu t - x_0]^2}{2\sigma^2 t}\right] - \exp\left[-\frac{2\mu(x_0 - x_b)}{\sigma^2}\right]\exp\left[-\frac{[x-\mu t - 2x_b + x_0]^2}{2\sigma^2 t}\right]\right\}, \tag{A4}$$

the probability that the particle does not cross the boundary at time t can be obtained as:

$$\begin{aligned} S(t) &= \int_{-\infty}^{x_b} p(x,t)dx, \\ &= \frac{1}{2}\left\{erfc\left[\frac{-x_b + x_0 + \mu t}{\sqrt{2t}\sigma}\right] - \exp\left[\frac{2\mu(x_b - x0)}{\sigma^2}\right] erfc\left[\frac{x_b - x_0 + \mu t}{\sqrt{2t}\sigma}\right]\right\}, \end{aligned} \tag{A5}$$

where $erfc$ denotes the complementary error function. Finally, the first hitting time distribution can now be obtained as:

$$\begin{aligned} f_{H_{x_b}}(t) &= -\frac{dS(t)}{dt}, \\ &= \sqrt{\frac{(x_b - x_0)^2}{2\pi\sigma^2 t^3}}\exp\left[-\frac{(\mu t - x_b + x_0)^2}{2\sigma^2 t}\right], \\ &\sim IG\left(\frac{x_b - x_0}{\mu}, \frac{(x_b - x_0)^2}{\sigma^2}\right) \end{aligned} \tag{A6}$$

[1] B. Heber and M. S. Potgieter, Space Sci. Rev. **127**, 117 (2007).
[2] M. Potgieter, Living Rev. Solar Phys. **10**, 3 (2013).
[3] M. S. Potgieter, Adv. Space Res. **60**, 848 (2017).
[4] M. J. Boschini, S. Della Torre, M. Gervasi, G. La Vacca, and P. G. Rancoita, Adv. Space Res. **62**, 2859 (2018).
[5] W. C. de Wet, T. C. Slaba, F. Rahmanifard, J. K. Wilson, A. P. Jordan, L. W. Townsend, N. A. Schwadron, and H. E. Spence, Life Sci. Space Res. (Amsterdam) **26**, 149 (2020).
[6] E. N. Parker, Planet. Space Sci. **13**, 9 (1965).
[7] L. J. Gleeson and W. I. Axford, Astrophys. J. **154**, 1011 (1968).
[8] H. Moraal, Space Sci. Rev. **176**, 299 (2013).
[9] N. Marcelli *et al.*, Astrophys. J. Lett. **925**, L24 (2022).
[10] K. Herbst, A. Kopp, B. Heber, F. Steinhilber, H. Fichtner, K. Scherer, and D. Matthiä, J. Geophys. Res. **115**, D00I20 (2010).
[11] M. Potgieter, Braz. J. Phys. **44**, 581 (2014).
[12] D. Bisschoff and M. S. Potgieter, Astrophys. Space Sci. **361**, 48 (2016).
[13] M. J. Boschini, S. D. Torre, M. Gervasi, D. Grandi, G. Jóhannesson, G. L. Vacca, N. Masi, I. V. Moskalenko, S. Pensotti, T. A. Porter, L. Quadrani, P. G. Rancoita, D. Rozza, and M. Tacconi, Astrophys. J. Suppl. Ser. **250**, 27 (2020).
[14] M. S. Potgieter, O. P. M. Aslam, D. Bisschoff, and D. Ngobeni, Physics **3**, 1190 (2021).
[15] C. Corti, V. Bindi, C. Consolandi, and K. Whitman, Astrophys. J. **829**, 8 (2016).
[16] J. Gieseler, B. Heber, and K. Herbst, J. Geophys. Res. **122**, 10,964 (2017).
[17] Z. Shen, H. Yang, P. Zuo, G. Qin, F. Wei, X. Xu, and Y. Xie, Astrophys. J. **921**, 109 (2021).
[18] I. Cholis, D. Hooper, and T. Linden, Phys. Rev. D **93**, 043016 (2016).
[19] M. Kuhlen and P. Mertsch, Phys. Rev. Lett. **123**, 251104 (2019).
[20] M. Zhang, Astrophys. J. **513**, 409 (1999).
[21] A. Kopp, I. Büsching, R. Strauss, and M. Potgieter, Comput. Phys. Commun. **183**, 530 (2012).
[22] Z. N. Shen, G. Qin, P. Zuo, and F. Wei, Astrophys. J. **887**, 132 (2019).
[23] X. Luo, M. Zhang, X. Feng, M. S. Potgieter, F. Shen, and G. Bazilevskaya, Astrophys. J. **899**, 90 (2020).
[24] M. Zhang, Astrophys. J. **510**, 715 (1999).
[25] J. R. Jokipii and E. N. Parker, Planet. Space Sci. **15**, 1375 (1967).
[26] R. D. Strauss, M. S. Potgieter, A. Kopp, and I. Büsching, J. Geophys. Res. **116**, A12105 (2011).
[27] A. Molini, P. Talkner, G. G. Katul, and A. Porporato, Physica (Amsterdam) **390A**, 1841 (2011).
[28] N. R. Sheeley, Y. M. Wang, S. H. Hawley, G. E. Brueckner, K. P. Dere, R. A. Howard, M. J. Koomen, C. M. Korendyke, D. J. Michels, S. E. Paswaters, D. G. Socker, O. C. St. Cyr, D. Wang, P. L. Lamy, A. Llebaria, R. Schwenn, G. M. Simnett, S. Plunkett, and D. A. Biesecker, Astrophys. J. **484**, 472 (1997).
[29] D. J. McComas, H. A. Elliott, J. T. Gosling, D. B. Reisenfeld, R. M. Skoug, B. E. Goldstein, M. Neugebauer, and A. Balogh, Geophys. Res. Lett. **29**, 1290 (2002).
[30] M. S. Potgieter, E. E. Vos, M. Boezio, N. De Simone, V. Di Felice, and V. Formato, Sol. Phys. **289**, 391 (2013).
[31] Z. N. Shen and G. Qin, Astrophys. J. **854**, 137 (2018).
[32] E. N. Parker, Astrophys. J. **128**, 664 (1958).
[33] M. S. Potgieter, J. A. Le Roux, and R. A. Burger, J. Geophys. Res. **94**, 2323 (1989).
[34] J. Raath, M. Potgieter, R. Strauss, and A. Kopp, Adv. Space Res. **57**, 1965 (2016).
[35] G. Qin and Z. N. Shen, Astrophys. J. **846**, 56 (2017).
[36] J. R. Jokipii and J. Kóta, Geophys. Res. Lett. **16**, 1 (1989).
[37] J. R. Jokipii and B. Thomas, Astrophys. J. **243**, 1115 (1981).
[38] J. Kota and J. R. Jokipii, Astrophys. J. **265**, 573 (1983).
[39] J. L. Raath, R. D. Strauss, and M. S. Potgieter, Astrophys. Space Sci. **360**, 56 (2015).
[40] J. W. Bieber, W. H. Matthaeus, C. W. Smith, W. Wanner, M.-B. Kallenrode, and G. Wibberenz, Astrophys. J. **420**, 294 (1994).
[41] A. Teufel and R. Schlickeiser, Astron. Astrophys. **397**, 15 (2002).
[42] G. Qin, Astrophys. J. **656**, 217 (2007).
[43] L. L. Zhao, L. Adhikari, G. P. Zank, Q. Hu, and X. S. Feng, Astrophys. J. **849**, 88 (2017).
[44] A. Shalchi, Space Sci. Rev. **216**, 23 (2020).
[45] N. E. Engelbrecht, F. Effenberger, V. Florinski, M. S. Potgieter, D. Ruffolo, R. Chhiber, A. V. Usmanov, J. S. Rankin, and P. L. Els, Space Sci. Rev. **218**, 33 (2022).
[46] M. D. Ngobeni, O. P. M. Aslam, D. Bisschoff, M. S. Potgieter, D. C. Ndiitwani, M. Boezio, N. Marcelli, R. Munini, V. V. Mikhailov, and S. A. Koldobskiy, Astrophys. Space Sci. **365**, 182 (2020).
[47] O. P. M. Aslam, D. Bisschoff, M. D. Ngobeni, M. S. Potgieter, R. Munini, M. Boezio, and V. V. Mikhailov, Astrophys. J. **909**, 215 (2021).
[48] J. Giacalone and J. R. Jokipii, Astrophys. J. **520**, 204 (1999).
[49] C. Corti, M. S. Potgieter, V. Bindi, C. Consolandi, C. Light, M. Palermo, and A. Popkow, Astrophys. J. **871**, 253 (2019).
[50] X. Song, X. Luo, M. S. Potgieter, X. Liu, and Z. Geng, Astrophys. J. Suppl. Ser. **257**, 48 (2021).
[51] N. Tomassetti, F. Barao, B. Bertucci, E. Fiandrini, J. L. Figueiredo, J. B. Lousada, and M. Orcinha, Phys. Rev. Lett. **121**, 251104 (2018).
[52] G. P. Zank, W. H. Matthaeus, J. W. Bieber, and H. Moraal, J. Geophys. Res. **103**, 2085 (1998).
[53] K. D. Moloto, N. E. Engelbrecht, and R. A. Burger, Astrophys. J. **859**, 107 (2018).
[54] E. Fiandrini, N. Tomassetti, B. Bertucci, F. Donnini, M. Graziani, B. Khiali, and A. Reina Conde, Phys. Rev. D **104**, 023012 (2021).
[55] W. R. Webber and M. S. Potgieter, Astrophys. J. **344**, 779 (1989).
[56] W. R. Webber, M. S. Potgieter, and R. A. Burger, Astrophys. J. **349**, 634 (1990).
[57] R. D. Strauss, M. S. Potgieter, I. Büsching, and A. Kopp, Astrophys. Space Sci. **339**, 223 (2012).
[58] M. D. Ngobeni and M. S. Potgieter, Adv. Space Res. **56**, 1525 (2015).